Spike and vortex formation in an impulsively-accelerated multiphase medium

C. Randall Truman[1], M. Anderson[2], P. Vorobieff[1], P. Wayne[1], C. Corbin[1], T. Bernard[1] & G. Kuehner[1]
[1]*Department of Mechanical Engineering, The University of New Mexico, Albuquerque, New Mexico, USA*
[2]*Illinoisrocstar LLC, Champaign, Illinois, USA*

Abstract

We present an experimental and numerical study of a complex flow that develops upon impulsive (shock) acceleration of a compressible multiphase medium. In the initial conditions, both diffuse density interfaces (gas-gas) and sharp density interfaces (gas-fluid) are present, with the fluid phase embedded within the gas in the form of small droplets. Our initial experiments failed to reveal some features prominent in the numerical simulations. For such occurrences, it is common practice to look for problems with the computational model or its implementation. In the case we present, however, the fault lay with a visualization technique that relied exclusively on visible-light Mie scattering from the droplets. A different visualization technique (laser-induced fluorescence) reveals that droplets do not follow some of the flow features forming after acceleration. The experiments and numerics we present cover Mach numbers ranging from 1.2 to 2.1, with characteristic Atwood number (dimensionless density ratio) of 0.5.

1 Introduction

Hydrodynamic instabilities that occur at the interface of fluids with different physical properties are of fundamental interest. For differences in fluid density, the Richtmyer-Meshkov Instability (RMI) [1, 2] occurs under impulsive acceleration, *e.g.*, when a shock crosses the density interface. After a short period of linear growth, perturbations grow nonlinearly with time after the shock passes through the interface. As secondary instabilities develop, the flow transitions to turbulence, producing complete mixing of the fluids. Mixing between two gases can be

WIT Transactions on Engineering Sciences, Vol 79, © 2013 WIT Press
www.witpress.com, ISSN 1743-3533 (on-line)
doi:10.2495/MPF130111

considered as a single-phase case of RMI. This case is most pertinent to the present study. Multiphase RMI develops when not only gases are present, but non-gaseous components (liquid or solid particles) participate in the flow evolution as well. To some extent, multiphase RMI is also relevant to the work described here, as a small volume fraction of fluid droplets is also present. Similar problems of interest (shock propagation through a combination of gases and non-gaseous inclusions) include coal dust explosions [3], supersonic combustion with fuel droplets [4], an interstellar gas or plasma with dust particles [5], and inertial confinement fusion (ICF) [6]. Far from behaving as passive tracers following the flow, particles or droplets can actually cause instability in the fluid after shock passage: this recently identified phenomenon is called a particle-lag instability (PLI) [7, 8]. It occurs due to variations in the average density resulting from nonuniform initial distribution of the non-gaseous phase. Flow morphology developing due to PLI is superficially similar to the one that would form in RMI-driven flow, but with some important differences (*e.g.*, no shock focusing).

The current work reports observations made while attempting to use micron- to submicron glycol particles as tracers for RMI studies involving gases with significantly different densities. This is a commonly used experimental diagnostic for RMI studies. While it is recognized that even such small particles may lag behind the gas phase after shock acceleration, the discrepancy is minimized by making the particles as small as is feasible. The tracer particles are illuminated by laser pulses so that Mie scattering of the visible light in seeded regions of the flow can be imaged by a high-resolution digital camera. Thus the particles must be small enough to follow the flow but large enough to be efficient Mie scatterers. A second experimental diagnostic used in the study is planar laser-induced fluorescence (PLIF). Pulses of UV light excite acetone that has been pre-mixed with the heavy gas (SF_6) that produces the density gradient with surrounding air. Both techniques employ laser sheets, with images representing flow in a horizontal plane at times corresponding to the laser pulses. Mie scattering and PLIF images can be collected in the same plane, so that evolution of the flow structure can be elucidated by both techniques simultaneously.

One of the primary purposes of our experiments is to establish quantitative benchmarks for validation of numerical techniques. The authors have reported direct comparison of the experiments with simulations preformed with a multiphase code SHAMRC [8, 9, 10]. Anderson *et al.* [10] demonstrated that careful modeling of initial conditions is required to reproduce experimental results. These comparisons were invaluable in understanding the particle-lag instability (PLI). Simulations have also been used to guide experiments in selecting initial conditions and in studying short-time and long-time behavior of the instabilities.

The current work was undertaken to examine discrepancies between numerical modeling and the primary experimental diagnostic, namely Mie scattering. PLIF, the second experimental diagnostic, was added to isolate the effects of particle lag since its tracer (acetone) is diffused throughout the heavy gas (SF_6). The morphology of images produced by Mie scattering and PLIF is examined to make

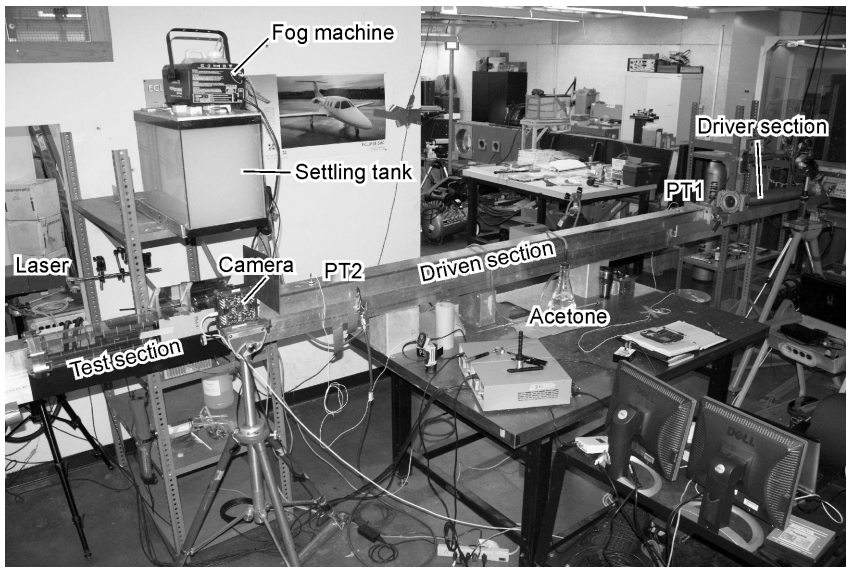

Figure 1: View of the experimental arrangement. Along with the components discussed in the text, components of the tracer injection system are labeled. Heavy gas (SF_6) is bubbled through Acetone, and the resulting mixture fills the Settling tank, into which glycol fog droplets produced by the Fog machine are also injected. Labels PT1 and PT2 refer to pressure transducers used to monitor the shock passage and trigger the image acquisition.

conclusions about the strengths and weaknesses of each diagnostic. The Mach number range is 1.2 to 2.1.

2 Experimental setup

Experiments were conducted at the UNM shock tube facility (Fig. 1). The shock is generated by pressurizing the driver section of the shock tube with helium gas and releasing a pressure wave into the driven section by puncturing the diaphragm that initially separates the pressurized driver section from the driven section, which at the beginning of the experiment is filled with quiescent air at ambient pressure. Downstream of the driven section is a transparent test section. Into the latter, a column of sulfur hexafluoride SF_6 pre-mixed with acetone and submicron- to micron-sized propylene glycol droplets is injected vertically. The injection is gravity-driven, the diameter of the injection nozzle is 6.35 mm. This injection produces an initially diffuse interface between the air and the material of the gas column, which moves with a velocity on the order of 1 m/s. The driven and test sections have a square cross-section, 7.62 cm on a side.

The density ρ_1 of the material that forms the seeded column is measured directly [10]. The dimensionless density difference (Atwood number) between the column and air (density ρ_1) is thus $A = (\rho_1 - \rho_2)/(\rho_1 + \rho_2) \approx 0.5$ in the experiments described here. Note that the Atwood number due to the contribution of the droplets alone would be ≈ 0.03, thus the dominant contribution to the density difference is the presence of SF_6 (nominal density 6.2 kg/m^3, about five times that of air). For a combination of pure SF_6 and air, the Atwood number would be 0.67, but in our experiments, SF_6 is mixed with acetone and a small fraction of air, leading to a slightly lower Atwood number. Accordingly, RMI due to this density difference is the instability that dominates the post-shock flow.

During experiments, laser pulses illuminate a horizontal plane in the test section, 3.81 cm above its bottom. In this plane, images of the flow are captured with an Apogee Alta camera with pixel resolution of 2048×2048 at 16 grayscale bits per pixel. Each camera exposure is produced by a train of four laser pulses, with visible-light (wavelength 532 nm) and ultraviolet (wavelength 266 nm) pulses alternating. Each pulse is about 5 ns in duration. The visible-light pulses produce Mie scattering off droplets, while the UV pulses produce visible-light fluorescence in acetone. Experiments were conducted at Mach numbers M ranging from 1.2 to 2.1. Here the Mach number is defined as $M = V_s/a$, where V_s is the velocity of the shock front and a is the speed of sound in ambient air.

3 Numerical setup

In the numerical modeling presented here, the injected column material was modeled as an ideal gas with density $\rho_1 = 3.675$ kg/m^3, and the gas constant $\gamma_1 = 1.4$, while the density and the gas constant of the surrounding air were defined as $\rho_2 = 1.225$ kg/m^3 and $\gamma_2 = 1.4$. These settings match the Atwood number ($A = 0.5$) measured in the lab. The initial distribution of density represented the diffusion on the interface between the column and the surrounding air as the gravity-driven heavy gas flows into the test section through a round nozzle [10].

The two-dimensional computational domain represented one half (with symmetry along the $x-$axis pointing streamwise) of the image plane visualized in experiment. The modeling was performed with SHAMRC [11], a second-order hydrodynamic automatic mesh refinement code that solves the conservation equations of fluid motion on an Eulerian grid. The latter can be adaptively refined. The solution of the governing equations is performed with a conservative, two-phase, operator-split, explicit, time-marching method that is second-order accurate in space and time. The equations are divided into Lagrangian and Eulerian terms, and their solution is accordingly split into two corresponding phases (phase 1 - Lagrangian, phase 2 - Eulerian). The energy redistribution terms are treated in a separate routine after the Lagrangian update, and before the Eulerian remap. In the case of the simulation presented here, the two-dimensional mesh was comprised of 6,000,000 zones, with a step of 0.005 cm in each direction. In the $y-$direction, the mesh extended from the $x-$axis (along the centerline of the shock tube) to the shock tube side wall.

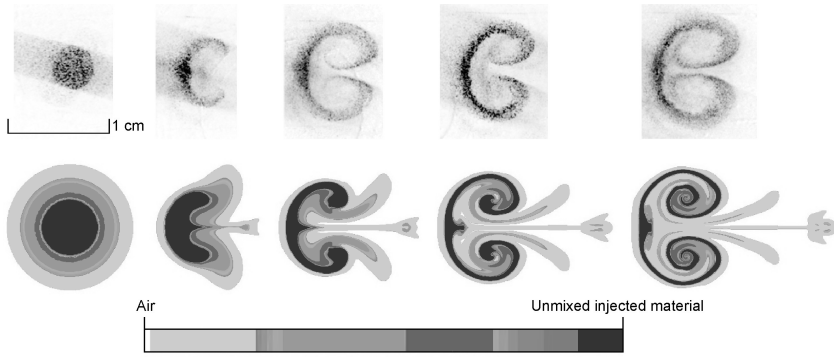

Figure 2: Comparison of flow visualization with glycol tracers (top) and numerical modeling (bottom) of Richtmyer-Meshkov instability developing in a heavy gas column with a cylindrical cross-section and an initially diffuse interface between the heavy gas and the surrounding light gas. Mach number is 1.7, Atwood number is 0.5. Shock direction is from left to right. The leftmost image in each row represents the initial conditions immediately before shock arrival from the left. Time intervals between subsequent dynamic images are 50 μs. Experimental images are inverted, so darker areas correspond to seeded flow.

To represent the shock wave arrival at the specific Mach number realized in experiment, high pressure and temperature air at a prescribed velocity was placed upstream of the initial conditions. These conditions were also fed in from the upstream domain boundary.

4 Comparison of results

As mentioned in the Introduction, one of the motivations for the present work was to understand the discrepancy between the results of experiments using glycol droplet tracers and numerical modeling similar to that described in the previous section. This discrepancy is illustrated by Fig. 2.

The simulation captures the dominant feature of the flow, the counter-rotating vortex pair that forms due to RMI. Moreover, the growth rates of this RMI-induced feature in experiment and in numerics are in good quantitative agreement. However, some numerical features are absent from the flow visualization images, namely the central spike that forms as a result of shock focusing in SF_6 and the "bunny ears" of material to each side of the spike. It was the authors' contention [10] that the modeling correctly identifies these features, but they cannot be visualized with Mie scattering off droplets because of two features of the tracer. First, in the initial conditions, SF_6 diffuses with the surrounding air, while the droplets don't. Second, upon shock acceleration, the tracer droplets lag behind the gaseous phase, exchanging momentum with it, until an equilibrium velocity is reached.

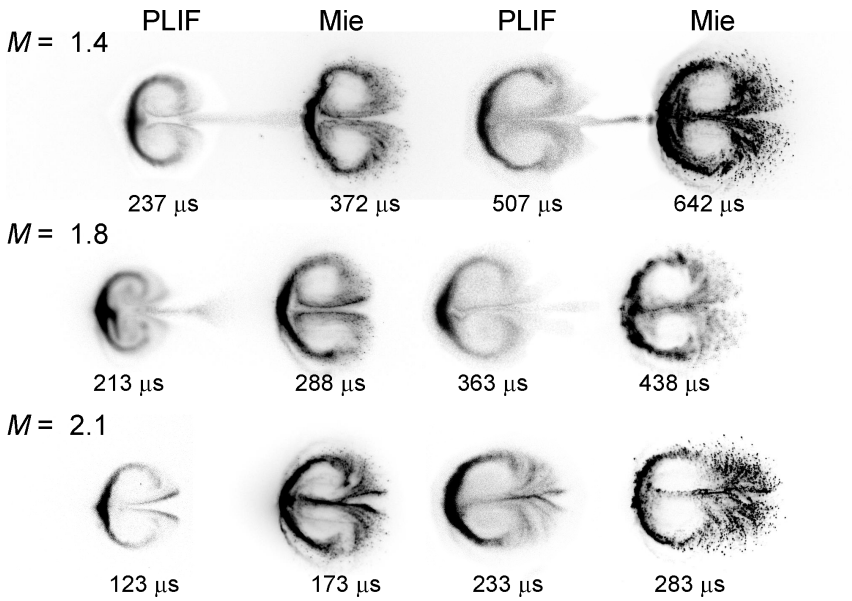

Figure 3: Experimental flow visualization using PLIF and Mie scattering off droplets for three Mach numbers. Flow direction is from left to right. Experimental images are inverted, so darker areas correspond to flow seeded with droplets (label "Mie") or marked with acetone tracer (label "PLIF"). Extent of imaged area is 10.09 cm. Individual image timings (with time $t = 0$ corresponding to shock reaching the center of the gas column) are labeled.

To confirm that the numerically observed features exist but are not followed by the droplets, we used a combination of visualization techniques (Fig. 3). The droplets are visualized by Mie scattering of visible light from laser pulses at 532 nm. The gaseous tracer (acetone) is visualized with planar laser-induced fluorescence (PLIF) from laser pulses at 266 nm. The pulses are staggered to highlight the differences between the features revealed by each technique.

The images shown here for three Mach numbers (1.4, 1.8, and 2.1, Fig. 3) were acquired at the same downstream position, so that the left edge of the imaged area was 3 cm downstream of the center of the initial conditions column. Each image contains four subsequent exposures, with odd exposures (first and third) produced by illuminating the visualization plane with the UV laser, and even exposures produced with the visible-light laser. As a result, in odd exposures, laser-induced fluorescence from acetone mixed with SF_6 is what visualizes the flow structures, and in even exposures, Mie scattering off droplets (same as in the experimental image in Fig. 2) is visible.

Both visualization techniques (PLIF and Mie scattering) show the counter-rotating vortex pair as the dominant feature of the post-shock flow. This vortex pair develops as the direct result of RMI from the planar shock interaction with the air-

seeded gas column density interface. However, PLIF visualization also manifests features not present in the Mie scattering images, specifically the central spike and the adjacent pair of "bunny ears." These features, while somewhat faint, are consistent with the numerical predictions – both in terms of overall morphology and in terms of the feature size and evolution. The droplet tracers are not present in the spike, the "bunny ears," and in the cores of the vortex pair, confirming the limitations of the flow-tracking fidelity suggested in previous research [10].

At the given downstream location, flow images for different Mach numbers appear remarkably similar, however, the actual timings at which the images were acquired differ considerably with M. The physical explanation of this phenomenon is rather simple. According to Richtmyer's linear theory [1], the initial instability growth rate is $v^{imp} = -\Delta U A k a_0$, where ΔU is the difference between the mean velocity of the density interface before and after the shock (in our case, the piston velocity with the negative sign), a_0 is the pre-shock amplitude of the initial interface perturbation, and k its characteristic wavenumber. This result for growth rates (although inaccurate for long-term description of the instability) allows us to introduce dimensionless time $\tau = 2kA|\Delta U|t$, where t is time after shock acceleration. For the same initial conditions and Atwood number, plotting the RMI amplitude as a function of τ would normalize the initial growth rate of RMI for different Mach numbers. Here it is easy to notice that τ would scale linearly, with no dependence on the Mach number, with downstream distance $x = |\Delta U|t$, namely $\tau = 2kAx$. Thus the dependence of the flow morphology evolution on the downstream distance (rather than time) is rather weak, as noted by many earlier researchers. However, our experiments make it possible to distinguish subtle features that change with M. For example, the "spike" clearly appears to lose its prominence with increasing Mach number.

5 Conclusions

We have performed a comparison of an experimental and a numerical study of shock-accelerated flow dominated by Richtmyer-Meshkov instability of a nominally two-dimensional, initially diffuse gas column. The study reveals that the discrepancy between experiments and numerics observed in earlier research owes its existence to the limitations of the diagnostic technique using small droplets to track the flow. The droplets do not behave as passive tracers upon shock acceleration, as they lag behind the gas flow. Moreover, the distribution of droplets in the initial conditions *prior* to the shock arrival is already likely to be different than the density distribution across the interface between the heavy-gas column and the surrounding ambient air.

Using a fluorescent gaseous tracer instead of droplets produces much better agreement between experimental results and numerics, with both the flow morphology and the feature growth rates being in good agreement. Likewise, explicit modeling of droplets as non-ideal tracers makes it possible to reproduce the experimentally observed droplet distribution numerically [10].

Future work should include a better experimental characterization of the initial conditions. A comparison between "pure" RMI (no droplet tracer) and a combination of RMI and PLI (the latter introduced by adding droplets) is also desirable.

Acknowledgement

This research is supported by the US National Nuclear Security Administration (NNSA) grant DE-FG52-10NA29648.

References

[1] R.D. Richtmyer. Taylor instability in shock acceleration of compressible fluids. *Communications in Pure and Applied Mathematics*, 13(2):297–319, 1960.

[2] E.E. Meshkov. Instability of the interface of two gases accelerated by a shockwave. *Izv. AN SSSR, Mekh. Zhidk. Gaza*, 4(5):151–157, 1969.

[3] V.P. Korobeinikov, I.V. Semenov, I.S. Menshov, R. Klemens, P. Wolanski, and P. Kosinski. Modelling of flow and combustion behind shock waves propagating along dust layers in long ducts. *Journal de Physique IV France*, 12:113–119, 2002.

[4] J. Yang, T. Kubota, and E.E. Zukoski. Applications of shock-induced mixing to supersonic combustion. *AIAA Journal*, 31(5):854–862, May 1993.

[5] P.K. Shukla. A survey of dusty plasma physics. *Physics of Plasmas*, 8:1791, 2001.

[6] V.N. Goncharov. Theory of the ablative Richtmyer-Meshkov instability. *Physical Review Letters*, 82:2091–2094, 1999.

[7] P. Vorobieff, M. Anderson, J. Conroy, R. White, and C.R. Truman. Vortex formation in a shock-accelerated gas induced by particle seeding. *Physical Review Letters*, 106:184503, 2011.

[8] P. Vorobieff, M. Anderson, J. Conroy, R. White, C.R. Truman, and S. Kumar. Analogues of Rayleigh-Taylor and Richtmyer-Meshkov instabilities in flows with nonuniform particle and droplet seeding. *Computational Methods in Multiphase Flow VI, eds. AA Mammoli, CA Brebbia, WIT Press, Southampton, UK*, pages 17–28, 2011.

[9] M. Anderson, P. Vorobieff, S. Kumar, J. Conroy, R. White, C. Needham, and C.R. Truman. Numerical simulation of a shock-accelerated multiphase fluid interface. In *Proceedings of 28th International Symposium on Shock Waves*, 2011.

[10] M. Anderson, P. Vorobieff, J. Conroy, C.R. Truman, R. White, and S. Kumar. An experimental and numerical study of shock interaction with a gas column seeded with droplets, 2013. Under consideration.

[11] J. Crepeau, C.E. Needham, and S. Hikida. Second Order Hydrodynamic Automatic Mesh Refinement Code (SHAMRC): Volume I, Methodology. Technical report, Applied Research Associates, Inc., May 2001.